



Preparation of the moon-white glaze by carbothermic reduction of Fe_2O_3 and SiC

Jianfeng Zhu, Pei Shi*, Fen Wang, Ting Zhao

School of Materials Science and Engineering, Shaanxi University of Science & Technology, Xi'an 710021, PR China



ARTICLE INFO

Article history:

Received 18 May 2015

Received in revised form 3 August 2015

Accepted 24 August 2015

Available online 2 September 2015

Keywords:

Moon-white glaze

Silicon carbide

Carbothermic reduction

Microstructure

Structural color

ABSTRACT

The moon-white glaze was successfully reproduced with the addition of 0.02 wt% silicon carbide (SiC) for supplying carbon (C) and reducing iron oxide (Fe_2O_3) at 1250 °C. Effects of the SiC contents on the chromaticity, precipitated phase and microstructure of moon-white glaze were investigated. Based on the analysis of colorimeter, XRD, XPS, FT-IR, SEM and TG-DSC, a possible coloring mechanism was proposed to explain the variation of glaze colors with the increasing of SiC content. The results indicated that the addition of SiC contributed to increasing the content of C and the size of phase separation droplets in glazes. The formation of C increased the ratio of Fe^{2+} to Fe^{3+} and the increased size of phase separation droplets weakened the structural color, which increased the L^* and b^* value of glazes. Therefore, the color of moon-white glaze got more blue and white gradually.

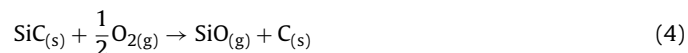
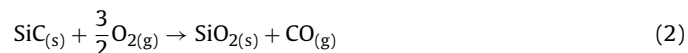
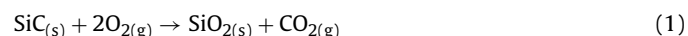
© 2015 Elsevier Ltd. All rights reserved.

1. Introduction

Celadon is one of the oldest color-glaze porcelain in China. A small amount of Fe_2O_3 acts as colorant in the glassy phase, and it is usually fired in reducing environment [1–3]. According to the depth of blue, the celadon glazes are classified into sky blue, bean green and moon-white glaze, etc. Especially, moon-white glaze has elegant color and jade-like appearance so that it is extremely prestigious in the entire world [4]. In recent years, for the coloring or other purpose, numerous modern ceramic and moon-white glaze or other celadon are still manufactured under a reduction environment, which not only raise the cost but also pollute the environment [5,6]. It is an urgent problem pressing for solution in the modern world.

In order to approach reduction flame under an oxidizing atmosphere, many efforts have been devoted to search efficient reducing agent in the past few decades. Metallic tin (Sn) was traditionally employed during the ancient age in the production of copper ruby glasses, and zinc (Zn) was also chosen because it presents lower oxidation activation energy, lying below copper oxides (CuO) in the Ellingham's diagram [7]. Nevertheless, these scarce and expensive materials not only increase the production cost, but also introduce impurity to the glass composition. Méar et al. investigated that titanium nitride (TiN) and SiC could be used as reducing agent of

containing lead oxide glasses to reduce lead (II) to metallic lead by the oxidation of TiN and SiC. Moreover, as a function of the temperature, SiC treatment of glasses gives more reduction of Pb(II) to Pb(0) than TiN treatment [8,9]. Based on the above, one can draw a conclusion that SiC is the strongest reducing agent of metal oxides than other reducing agents such as Sn, Zn and TiN at high temperature. The related reactions of the SiC oxidation are shown in Eqs. (1)–(4), in which, Eqs. (1)–(2) are the passive oxidation and Eqs. (3)–(4) are the active oxidation at higher temperatures [10–12].



Accordingly, some scholars suggested that the addition of SiC to a glaze provided a reducing agent within the glaze itself, or a "local" reducing agent [6]. However, until now, seldom studies have been made to prepare celadon glaze with reducing agents. In this work, SiC was utilized as the reducing agents to reduce Fe_2O_3 and reproduce the moon-white glaze in an oxidizing environment. In order to better control glaze color, the effects of SiC contents on the evolution of crystalline phase and phase separation of the moon-white glaze were investigated in detail. The coloring changing mechanism about the moon-white glaze color was also discussed.

* Corresponding author. Fax: +86 2986168188.

E-mail addresses: zhujf@sust.edu.cn (J. Zhu), shipei7121@163.com (P. Shi).

Table 1

Chemical compositions of the raw materials (wt%).

Raw materials	SiO ₂	Al ₂ O ₃	Fe ₂ O ₃	CaO	MgO	K ₂ O	Na ₂ O	SiC	Ca ₃ (PO ₄) ₂
Feldspar	69.94	17.41	0.51	3.54	1.01	0.51	7.08	–	–
Quartz	98.37	1.41	0.22	–	–	–	–	–	–
Calcite	0.67	–	–	98.68	0.65	–	–	–	–
Talc	64.64	–	0.06	0.24	34.96	0.06	0.04	–	–
Calcium phosphate	–	–	–	–	–	–	–	–	99.9
Silicon carbide	–	–	0.50	–	–	–	–	98.5	–

2. Experimental

2.1. Glaze preparation

The base glaze compositions were made by 58.8 wt% of Na-feldspar, 29.4 wt% of quartz sand, 7.8 wt% of calcite, 2 wt% of talc, 2 wt% of calcium phosphate (Ca₃(PO₄)₂). Meanwhile, SiC was added as the reducing agent and commercial grade Fe₂O₃ was added as the colorant, the addition amount of them were 0–0.1 wt% and 0.2 wt% of the base glaze, respectively. Chemical compositions of the raw materials are given in Table 1.

The raw glaze slurry was prepared by directly milling the starting materials which was weighted before with 75 wt% water, 0.8 wt% sodium carboxyl methyl cellulose (CMC), 0.3 wt% sodium tripolyphosphate (STP) and milled at a rate of 300 r/min for 35 min. The glaze slip was sieved and the density was adjusted to 1.5 g/cm³ by water. Then the glaze slip was applied to the biscuits test piece (\varnothing 4–5 cm) by dipping. After dried, the test pieces were fired at a heating rate of 3 °C/min to 900 °C and 1.5 °C/min to 1250 °C, and then insulated for 40 min at this temperature under an oxidizing atmosphere. Finally, the samples were cooled down to room temperature naturally in the furnace.

2.2. Characterization

The color parameters (L^* , a^* , b^*) for the fired specimens were measured using the WSD-3C colorimeter. And the phase composition of the test pieces was identified by X-ray diffraction (XRD) using a D/max 2200PC X-ray diffractometer (Japan) with Cu K α radiation ($\lambda = 1.5406 \text{ \AA}$). Meanwhile the samples were measured at a scanning rate of 8 °/min in the 2 θ range of 10–60° under 40 kV and 100 mA. The chemical analysis was performed on an ESCALAB MKII X-ray photoelectron spectrometer (VG Scientific, UK) using Al K α radiation. The infrared spectra at 400–1200 cm⁻¹ were characterized by a Spectrum One FT-IR spectrometer (VERTE70) and the KBr standard pellet method. The microstructure of the samples was investigated by scanning electron microscopy (SEM) equipped with energy dispersive spectrometry (EDS). Before the testing, the surface of the samples was etched using 10 vol% HF for 30 s to expose the crystals and phase separation structures. The thermal analysis of samples was carried out with a thermal analyzer (NETZSCH STA 409 PC/PG, Selb, Germany) from ambient temperature to 1250 °C at a heating rate of 10 °C/min under oxygen atmosphere.

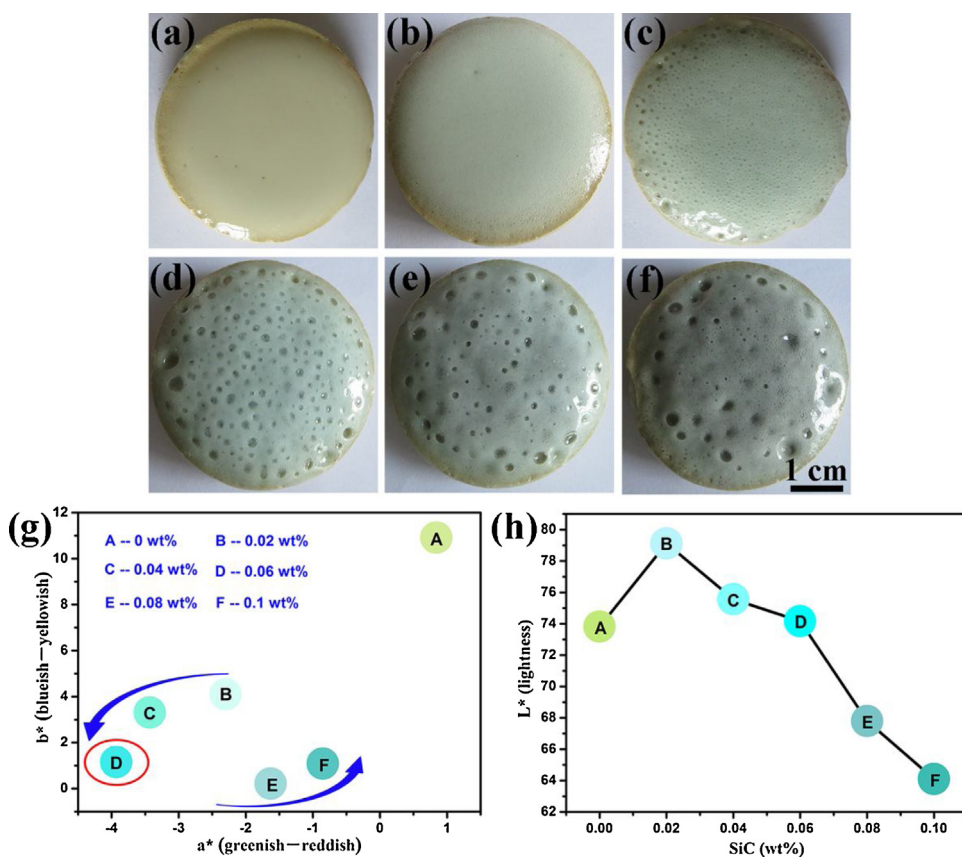


Fig. 1. Appearance of glazes, (a)–(f) different SiC contents of 0, 0.02, 0.04, 0.06, 0.08 and 0.1 wt%; (g,h) quantitative analysis of color tone for samples, (g) Plots of a^* and b^* values, (h) L^* values as a function of SiC contents.

3. Results and discussion

Fig. 1(a–f) shows the appearance of the typical glaze containing 0–0.1 wt% SiC. As being observed, the bubbles appeared on the glaze surfaces when SiC content was more than 0.02 wt% and the sizes increased with increasing the SiC content, which was ascribed to the oxidation of SiC at high temperature (see Eqs. (1)–(4)) [10–12]. And the color tone of the glazes systematically changed (**Fig. 1(g and h)**). **Fig. 1(g)** shows a^* and b^* values of the glazes with different SiC contents. It could be found that the glaze without SiC addition exhibited the highest a^* and b^* values. **Fig. 1(h)** shows the variation of L^* as a function of SiC contents. L^* values presented local maxima with 0.02 wt% SiC, and decreased with increasing of the SiC content (**Fig. 1(h)**). Glazes with addition of 0.02, 0.04, and 0.06 wt% SiC displayed the most vivid color, exhibited almost the same L^* , a^* , and b^* values as the moon-white glaze color. Combining the performance of glaze surfaces, the SiC content was determined to be 0.02 wt% in the moon-white glaze.

X-ray diffraction (XRD) patterns of glazes with 0, 0.02, 0.06 and 0.1 wt% SiC contents, are shown in **Fig. 2**, respectively. The characteristic amorphous hump could be seen within the $2\theta \approx 15\text{--}35^\circ$ range in all samples, which were associated to a large amount of aluminosilicate glass [13]. Meanwhile, some weak peaks were corresponding to the presence of quartz with characteristic peak at 26.24° and carbon with characteristic peak at 26.60° crystallization. Among them, the quartz existed in every sample and carbon only existed in SiC-containing samples. So the quartz was likely to be from the starting composition, while the carbon phase was formed from the oxidation of SiC (see Eq. (3)). Also, the content of carbon increased with increasing the SiC contents. Accordingly, a^*

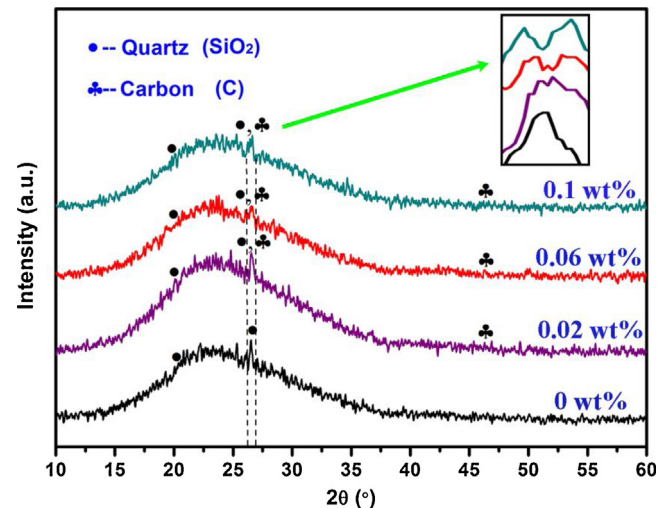


Fig. 2. XRD patterns of glazes with different SiC contents. Insets are enlarged images.

and b^* value of glazes increased when the SiC content was more than 0.06 wt%.

Fig. 3 displays the SEM images and EDS analysis of the etched glaze surface containing 0.1 wt% SiC. It can be clearly seen that a large number of aggregate crystals disorderly distributed in glass matrix (**Fig. 3(a)**). **Fig. 3(b)** shows that lamellar structures on the surface were presented due to acid treatment. The chemical composition of crystals was analyzed by EDS in **Fig. 3(c)** and (d), measured on the microspots denoted by the positions 1 and 2 in the SEM

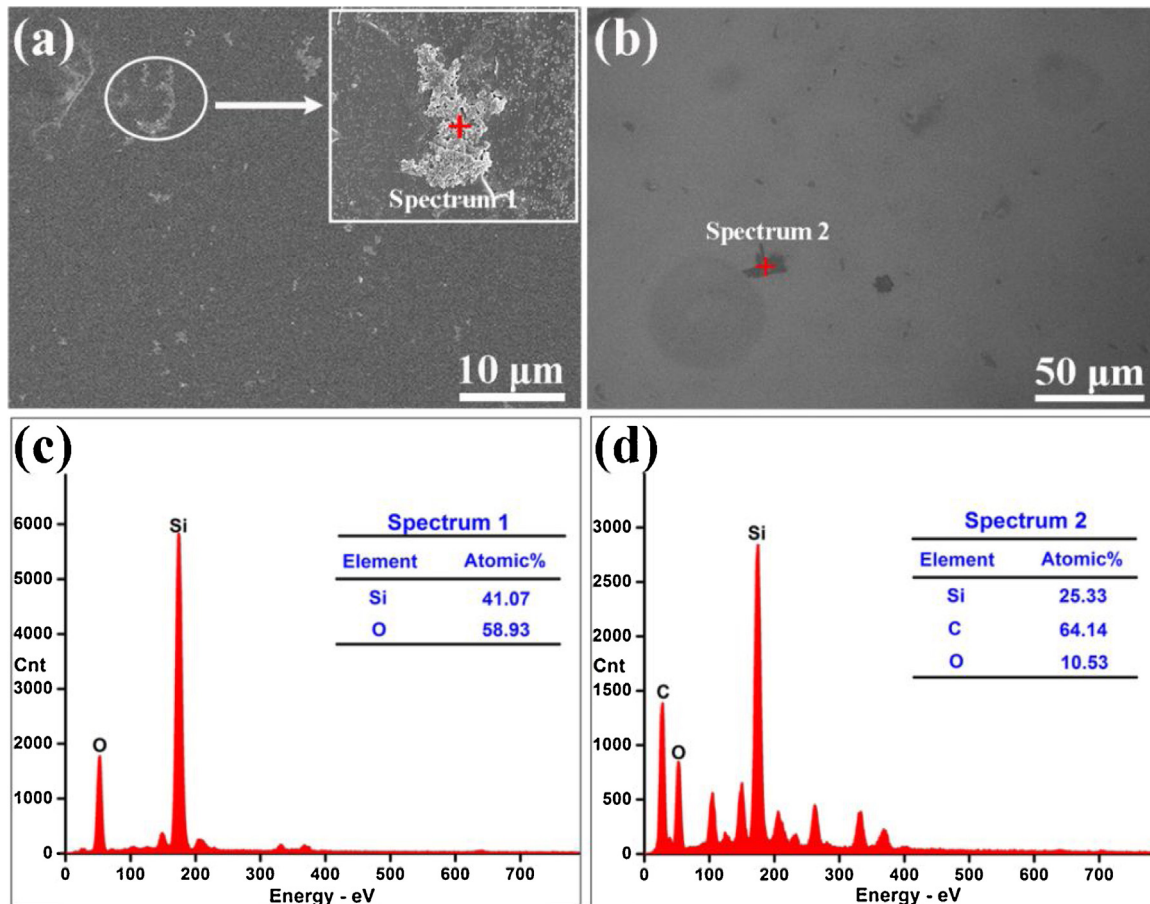


Fig. 3. (a) and (b) SEM images of crystals on the glaze surface with 0.1 wt% SiC; (c) and (d) EDS spectra.

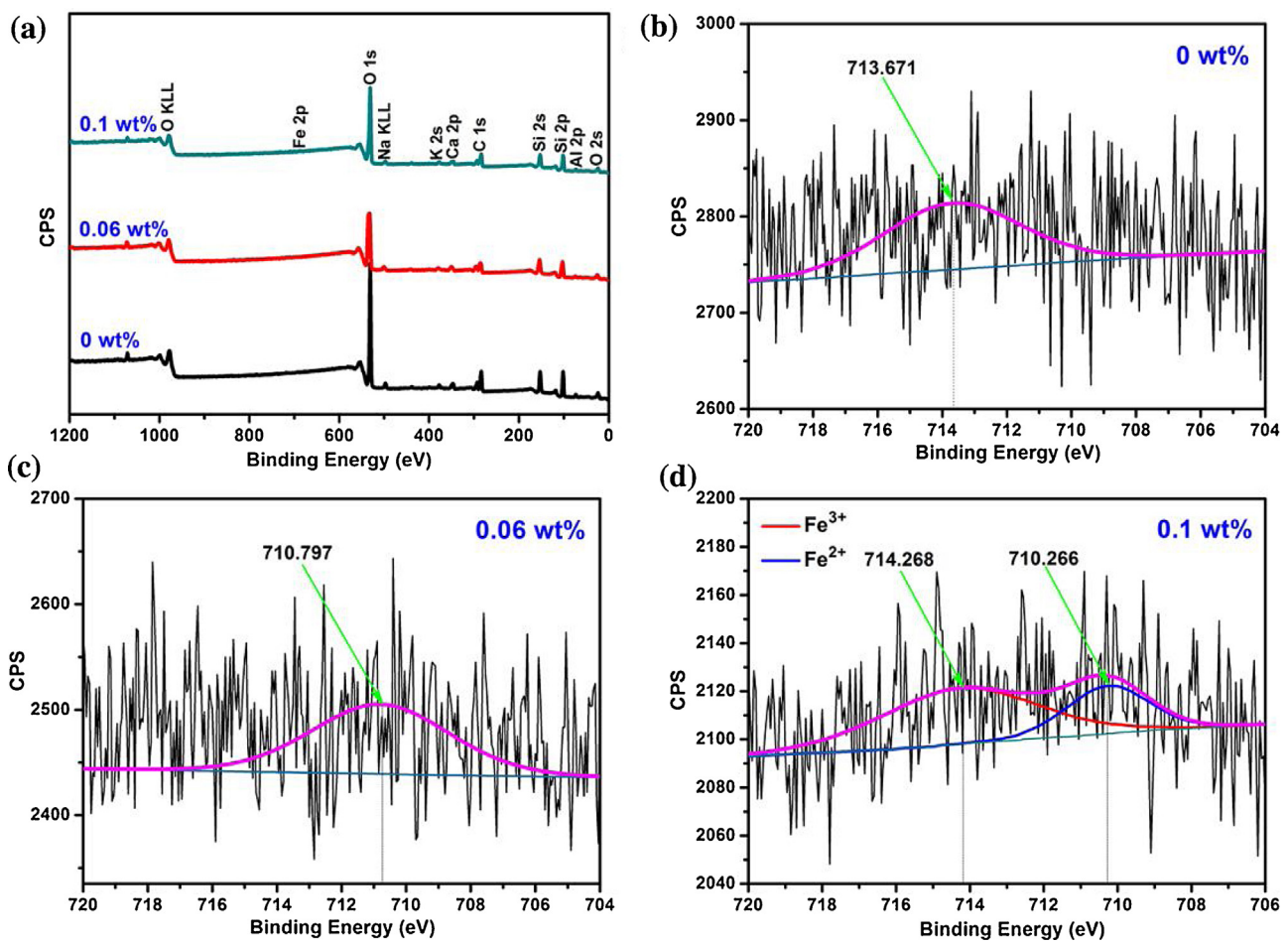


Fig. 4. (a) XPS survey spectra, (b)–(d) fitting spectra of the Fe2p 3/2 peaks of the glazes with different SiC contents.

Table 2
Glazes compositions synthesized and compared with XPS analyses.

	Atomic%		
	O 1s	C 1s	Si 2p
0 wt% SiC	60.17	15.02	24.82
0.06 wt% SiC	58.34	16.36	25.30
0.1 wt% SiC	50.22	29.50	20.28

images of crystals. It showed that the crystal in position 1 was rich in Si and O, whereas the crystal in position 2 was rich in C. Combining with the XRD analysis in Fig. 2, position 1 was the residue quartz which formed a big aggregate (Fig. 3(a)), while position 2 was nearly lamellar carbon (Fig. 3(b)). The results further indicated that the glazes surface got black, which was due to the crystalline effect of carbon. The glass phase in glaze was continuous and dense; thus it could have the excellent physical and chemical protective function of avoiding oxidation of the C in an oxygen atmosphere.

The XPS technique is a good analytical tool for elemental analysis, as the binding energy (BE) values of core levels are, to a certain extent dependent on the molecular environment [14]. Hence the stoichiometry of the SiC glazes was analyzed by using XPS. Typical broad-scan XPS spectra of the 0 wt%, 0.06 wt% and 0.1 wt% SiC glazes within the BE range of 0–1200 eV are shown in Fig. 4. As expected, the three spectra had similar spectral features and peak positions, since the chemical status of the elements in both cases was the same. Furthermore, the presence of O 1s, C 1s and Si 2p signal could be noted, both related to reduction degree of glaze. Table 2 shows O, C and Si concentrations of glazes with different SiC contents.

For comparison, a significant decrease of the O content accompanied by an increase of C concentration could be observed, and the Si concentration was kept essentially constant with the increasing of SiC content. Obviously, reduction degree of these samples was increased.

The broad Fe 2p3/2 peaks suggested the coexistence of Fe^{2+} and Fe^{3+} in samples [15]. Fig. 4(b)–(d) shows the fitting spectra of Fe 2p3/2 peaks obtained from the samples with different SiC contents, where the binding peaks were fitted by Lorentzian–Gaussian functions. It was found that the Fe 2p3/2 peak was shifted to higher binding energies side, so Fe^{2+} concentration increased with the increasing of SiC content. When the content of SiC was 0.1 wt%, The Fe^{2+} to Fe^{3+} atomic ratios of glaze was 68.84/31.16. Therefore, the XPS results further confirmed that the SiC was helpful to increase the Fe^{2+} concentration in glazes, which could make glaze colors turn blue gradually.

The IR absorbance spectra of investigated glazes are illustrated in Fig. 5. All the spectra showed four characteristic peaks located at 1070 cm^{-1} , 784 cm^{-1} , 615 cm^{-1} and 465 cm^{-1} , respectively. The absorption band at 1070 cm^{-1} was assigned to the stretching vibration of Si–O, which indicated that the structure of the tested glazes was dominated by the so-called Q³ group (where Q is the number of bridging oxygen) [16,17]. The band at 784 cm^{-1} could be linked with bending vibrations of two types of bridge bonds Si–O–Si and Si–O–Al, while the band at 465 cm^{-1} was associated with bending vibrations of O–Si–O. Presence of a small band at 615 cm^{-1} should be linked with the presence of Si– and Si–O rings [17]. Comparing decomposition of studied glazes, the intensity of all characteristic bands was all increased with the increase of SiC content. It could be

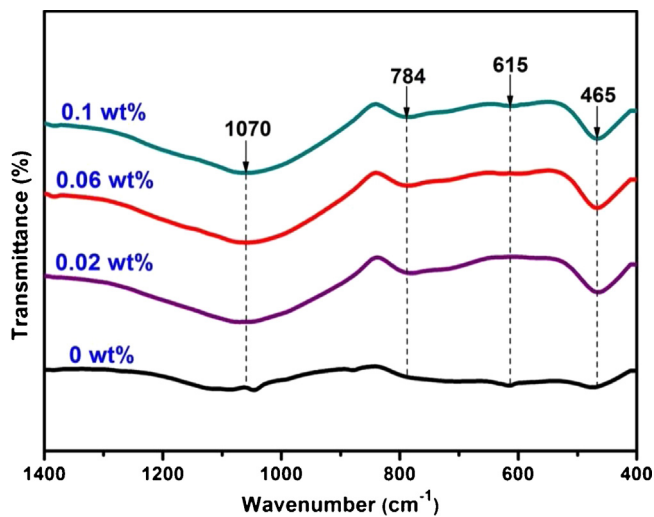


Fig. 5. FT-IR spectrum of the glazes with different SiC contents.

concluded that the addition of SiC led to $(\text{SiO}_4)^{4-}$ tetrahedra break in the moon-white glazes, which destroyed the covalent amorphous network. As a result, the viscosity of molten glazes decreased with the increasing of SiC content.

Fig. 6(a-d) presents the SEM micrographs of etched glaze surfaces containing different SiC contents of 0 wt%, 0.02 wt%, 0.06 wt% and 0.1 wt%. It can be shown that the discrete droplet phase separation structures were formed in every glaze surface [18]. **Fig. 6(e)** displays the SEM micrograph of the fracture surface of the glaze with adding 0.1 wt% SiC. It was obviously seen that the phase separation droplets located in all over the glaze. Consequently, it could be proved that the phase separation occurred on the whole samples (with 0–0.1 wt% SiC). Additionally, with the increase of SiC content, the average diameter of phase separation droplets increased and the density decreased in the glazes. The reason for this was that, the viscosity of molten glazes decreased when the content of SiC was increased. Therefore, the movement speed of particles got faster so that discrete phase droplets were easy to move to the surface of phosphate glass [19,20].

The structural colored glaze consisting of discrete droplet phase separation structures showed structural color developed by the Rayleigh scattering. When the average diameter of scattering ions was 1–100 nm, the Rayleigh scattering might occur on glaze surface. The scattering intensity was determined with the following formulas [21–24].

$$I(\lambda)_{\text{scattering}} \propto \frac{I(\lambda)_{\text{incident}}}{\lambda^4} \quad (5)$$

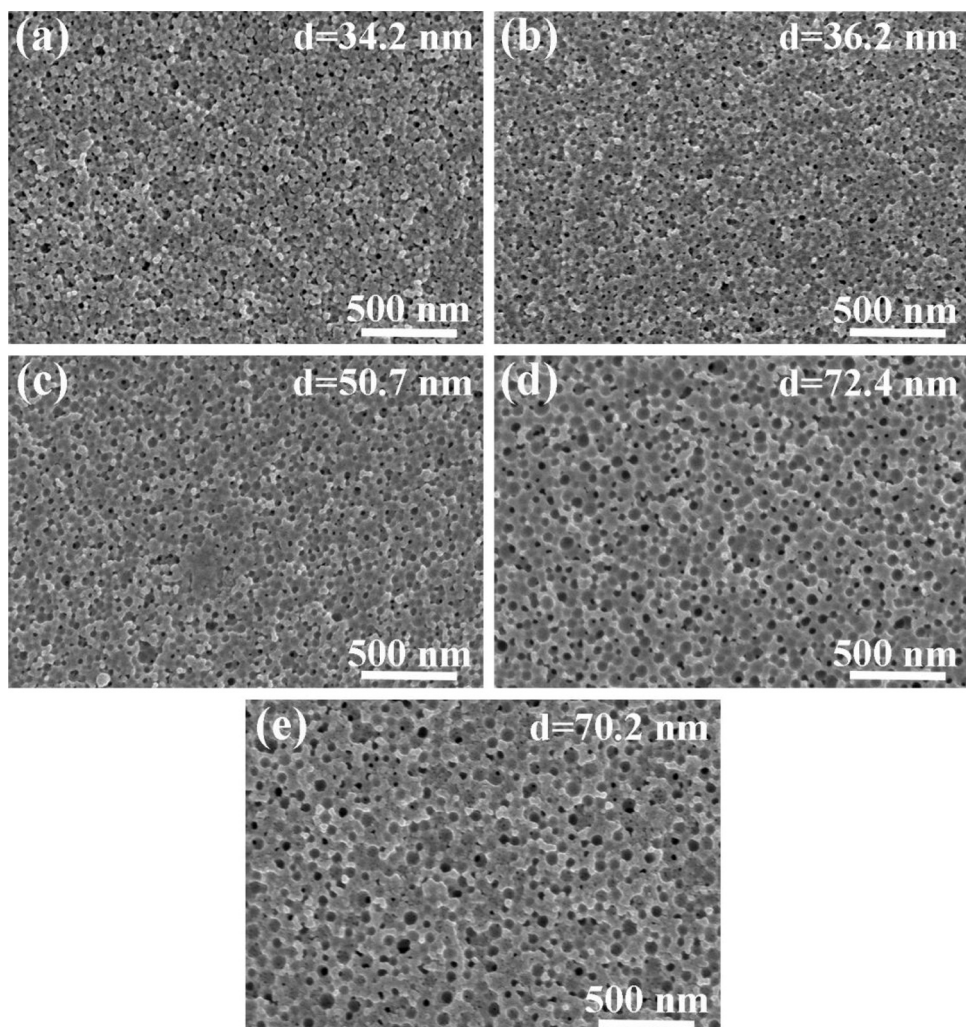


Fig. 6. Typical SEM images of separation structure on the glaze surfaces, (a)–(d) different SiC contents of 0, 0.02, 0.06 and 0.1 wt%; (e) SEM micrograph of the typical fracture surface of the glaze with adding 0.1 wt% SiC.

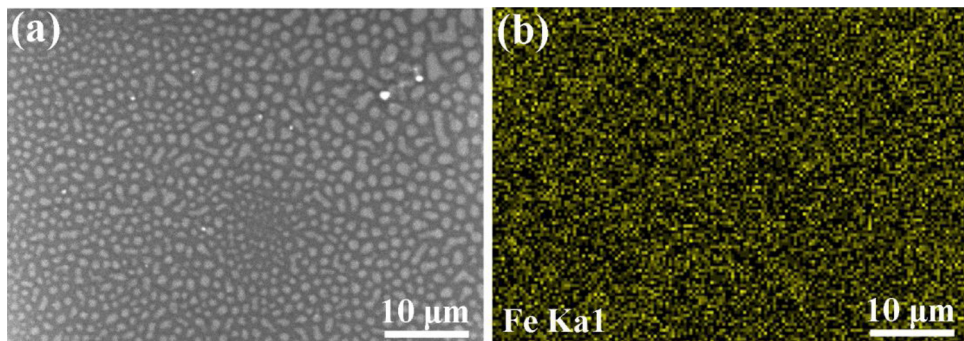


Fig. 7. SEM-BSE image and corresponding EDS elemental mapping image of Fe Ka1 for the unetched glaze surface with 0.1 wt% SiC, (a) SEM-BSE image; (b) EDS elemental mapping image.

where $I(\lambda)_{\text{incident}}$ and λ are intensity and wavelength of the incident and light, respectively. The smaller the λ , the easier the Rayleigh scattering. Because blue light is at the short wavelength end of the visible spectrum, it is scattered in the atmosphere much more than the longer-wavelength red light. As a result, the structural color developed by the Rayleigh scattering showed blue and the glaze colors became blue with addition of calcium phosphate. When the average diameter of phase separation droplet was bigger, the scattering intensity ($I(\lambda)_{\text{incident}}$) was less and the opalescence blue which was formed by structural color was lighter. Therefore, the glaze colors got more blue and white gradually with the increasing of Fe^{2+} concentration in the glazes.

Since the structural color was greatly influenced by the position of Fe in the glazes, it was necessary to clarify where the $\text{Fe}^{3+}/\text{Fe}^{2+}$ located in the glass matrix or in the droplets. Fig. 7 displays the SEM-BSE and corresponding EDS elemental mapping image of Fe Ka1 for the unetched glaze surface with addition of 0.1 wt% SiC. From Fig. 7(a), it was found that the oil-drop phase separation droplets uniformly distributed in the glass matrix. As shown in Fig. 7(b), the whole glaze surface contained the element Fe with basically uniform distribution density, conforming that the element Fe did not only gather in the glass matrix but also in the droplets. The reason for this was that, the small amount of (0.2 wt%) of Fe_2O_3 was not enough to cause the element composition difference of Fe between glass matrix and droplets [25]. Consequently, the refractive indices between base phase and phase separation droplets were very small in the samples. Meanwhile, the structural color could not be greatly affected by adding the small amount of Fe_2O_3 [21].

Thermo gravimetric (TG) analysis and differential scanning calorimetry (DSC) analysis are used to study weight change and all the transformations during a heating cycle. The TG–DSC curves of the glaze with 0.1 wt% SiC are presented in Fig. 8. An initial weight loss was observed in the TG curve which was attributable to the removal of residual water and the combustion of the organic matter. And then, two small endothermic peaks at about 454.0 °C and 692.1 °C were attributed to the removal constitution water accompanied by mass loss. At higher temperatures, a slow weight loss was corresponding to the decomposition of calcite. Meanwhile, there was an exothermic peak at about 1137.7 °C. Some workers attributed this reaction to the decomposition of feldspar while oth-

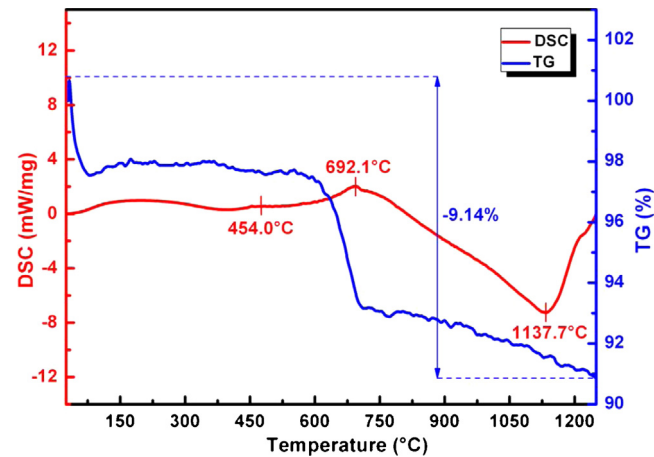
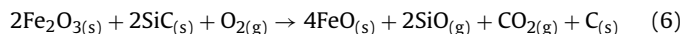


Fig. 8. DSC–TG curves of investigated glaze.

ers attributed it to SiC oxidation and reduction reaction of Fe_2O_3 by C [6,26]. So, the formation temperature of FeO was 1137.7 °C in this work. The main reaction is expressed by Eq. (6) as following:



Consequently, a reaction mechanism of carbothermic reduction of Fe_2O_3 by SiC for the moon-white glaze preparation could be proposed on the basis of above experimental results. The process of reaction was described as follows: when the excessive amount of SiC was added to the base glaze, it was passively oxidized by air in the furnace and formed CO and C at 1137.7 °C (see Eqs. (3) and (4)). And then as the colorant for moon-white glaze, Fe_2O_3 was reduced to FeO by generating CO and C (see Eq. (6)) as well as the unreacted C was in the glazes. After cooling, the glazes were moon-white color when the SiC contents were 0.02–0.06 wt%, and the glazes with 0.08–0.1 wt% SiC got green-black color because of the residual C. Fig. 9 shows the possibly reactions on the glaze surfaces.

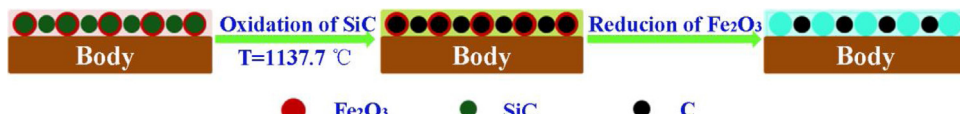


Fig. 9. Proposed mechanism of the carbothermic reduction of Fe_2O_3 by SiC on the moon-white glaze preparation.

4. Conclusions

The moon-white glaze was successfully reproduced with the addition of 0.02 wt% SiC under an oxidizing environment. With increasing of the SiC content, C was formed so that Fe_2O_3 reduced while the ratios of Fe^{2+} to Fe^{3+} in glazes increased. The SEM microstructure showed that the discrete droplet phase separation structures were developed in glazes and their sizes were less than 100 nm, so the structural color was formed owing to the Rayleigh scattering. A dual coloring changing mechanism with the increasing of the SiC content was in effect for the moon-white glaze, covering the carbothermic reduction and the varying size of phase separation droplets.

Acknowledgements

This work was supported by the National Foundation of Natural Science, China (51472153), the Key Project of State Administration of Culture Heritage, China (20120218), Research and Application of Ceramic Glaze Prepared with Mineral Waste Residue, China (2012KTDZ02-01-03), and the Graduate Innovation Fund of Shaanxi University of Science and Technology.

References

- [1] Jong-Young Kim, Hyunggoo No, A. Young Jeon, Ungsoo Kim, Jae-Hwan Pee, Woo-Seok Cho, Kyung Ja Kim, Chin Mo Kim, Chul Sung Kim, Mössbauer spectroscopic and chromaticity analysis on colorative mechanism of celadon glaze, *Ceram. Int.* 37 (2011) 3389–3395.
- [2] J.Z. Li, History of Ancient Science and Technology (Ceramics Part), Science Press, Beijing, 1998.
- [3] W.D. Li, J.Z. Li, J. Wu, J.K. Guo, Study on the phase-separated opaque glaze in ancient China from Qionglai kiln, *Ceram. Int.* 29 (2003) 933–937.
- [4] Julian P. Julian, Kenneth H. Tonge, Reduction processes in the formation of lustre glazed ceramics, *Thermochim. Acta* 340–341 (1999) 395–405.
- [5] B. Zhang, Z.Y. Gao, W.J. Zhao, G.X. Li, H.S. Cheng, Z.Q. Zhang, Mössbauer spectroscopy and neutron activation analysis of ancient Chinese glazes, *Appl. Clay Sci.* 25 (2004) 161–165.
- [6] Allen A. Denio, The joy of color in ceramic glazes with the help of redox chemistry, *J. Chem. Educ.* 10 (2001) 1298–1304.
- [7] A. Quaranta, R. Ceccato, C. Menato, L. Pederiva, N. Capra, R. Dal Maschio, Formation of copper nanocrystals in alkali-lime silica glass by means of different reducing agents, *J. Non-Cryst. Solids.* 345&346 (2004) 671–675.
- [8] F. Méar, P. Yot, M. Cambon, M. Ribes, The changes in lead silicate glasses induced by the addition of a reducing agent (TiN or SiC), *J. Non-Cryst. Solids* 351 (2005) 3314–3319.
- [9] Pascal G. Yot, François O. Méar, Lead extraction from waste funnel cathode-ray tubes glasses by reaction with silicon carbide and titanium nitride, *J. Hazard. Mater.* 172 (2009) 117–123.
- [10] X.Z. Cheng, Y.H. Wang, Y.Q. Liang, J.B. Zang, J. Lu, Y.Q. Yu, X.P. Xu, Avoiding the oxidation of SiC in SiC-borosilicate glass composites by adding zinc, *Corros. Sci.* 90 (2015) 413–419.
- [11] X.Z. Cheng, Y.H. Wang, Y.Q. Liang, J.B. Zang, J. Lu, Y.Q. Yu, X.P. Xu, Promoting oxidation-resistance property of SiC particles by adding Ti powder into SiC-borosilicate glass composites, *Mater. Lett.* 134 (2014) 34–37.
- [12] M. Villegas, T. Sierra, F. Lucas, J.F. Fernández, A.C. Caballero, Oxidation treatments for SiC particles and its compatibility with glass, *J. Eur. Ceram. Soc.* 27 (2007) 861–865.
- [13] X.S. Cheng, S.J. Ke, Q.H. Wang, H. Wang, A.Z. Shui, P.A. Liu, Characterization of transparent glaze for single-crystalline anorthite porcelain, *Ceram. Int.* 38 (2012) 4901–4908.
- [14] H.W. Nesbitt, G.M. Bancroft, G.S. Henderson, R. Ho, K.N. Dalby, Y. Huang, Z. Yan, Bridging, non-bridging and free (O^{2-}) oxygen in $\text{Na}_2\text{O}-\text{SiO}_2$ glasses: an X-ray photoelectron spectroscopic (XPS) and nuclear magnetic resonance (NMR) study, *J. Non-Cryst. Solids* 357 (2011) 170–180.
- [15] Toru Yamashita, Peter Hayes, Analysis of XPS spectra of Fe^{2+} and Fe^{3+} ions in oxide materials, *Appl. Surf. Sci.* 254 (2008) 2441–2449.
- [16] Ishu Kansal, Ashutosh Goel, U. Dilshat Tulyaganov, Raghu Raman Rajagopal, M.F. José Ferreira, Structural and thermal characterization of $\text{CaO}-\text{MgO}-\text{SiO}_2-\text{P}_2\text{O}_5-\text{CaF}_2$ glasses, *J. Eur. Ceram. Soc.* 32 (2012) 2739–2746.
- [17] Janusz Partyka, Maciej Sitarz, Magdalena Leśniak, Katarzyna Gasek, Piotr Jeleń, The effect of $\text{SiO}_2/\text{Al}_2\text{O}_3$ ratio on the structure and microstructure of the glazes from $\text{SiO}_2-\text{Al}_2\text{O}_3-\text{CaO}-\text{MgO}-\text{Na}_2\text{O}-\text{K}_2\text{O}$ system, *Spectrochim. Acta A* 134 (2015) 621–630.
- [18] Encarna Bou, Arnaldo Moreno, Agustín Escardino, Ana Gozalbo, Microstructural study of opaque glazes obtained from frits of the system: $\text{SiO}_2-\text{Al}_2\text{O}_3-\text{B}_2\text{O}_3-(\text{P}_2\text{O}_5)-\text{CaO}-\text{K}_2\text{O}-\text{TiO}_2$, *J. Eur. Ceram. Soc.* 22 (2007) 1791–1796.
- [19] Francisco Jose Torres, Javier Alarcón, Pyroxene-based glass-ceramics as glazes for floor tiles, *J. Eur. Ceram. Soc.* 25 (2005) 349–355.
- [20] W.D. Kingery, P.B. Vandiver, I.W. Huang, Y.M. Chiang, Liquid-liquid immiscibility and phase separation in the quaternary systems $\text{K}_2\text{O}-\text{Al}_2\text{O}_3-\text{CaO}-\text{SiO}_2$ and $\text{Na}_2\text{O}-\text{Al}_2\text{O}_3-\text{CaO}-\text{SiO}_2$, *J. Non-Cryst. Solids* 54 (1983) 163–171.
- [21] Shuichi Kinoshita, Shinya Yoshioka, Structural colors in nature: the role of regularity and irregularity in the structure, *ChemPhysChem* 6 (2005) 1442–1459.
- [22] Kenji Higashiguchi, Masafumi Inoue, Tomohiro Oda, Kenji Matsuda, Solvent-responsive structural colored balloons, *Langmuir* 28 (2012) 5432–5437.
- [23] Ryan Thalman, Kyle J. Zarzana, Margaret A. Tolbert, Rainer Volkamer, Rayleigh scattering cross-section measurements of nitrogen, argon, oxygen and air, *J. Quant. Spectrosc. Radiat. Transf.* 147 (2014) 171–177.
- [24] F. Wang, H.J. Luo, Q. Li, W.D. Li, Characteristic and coloring mechanism of the separative-phase colored ceramic, *J. Chin. Ceram. Soc.* 37 (2009) 181–186.
- [25] X.Q. Chen, R.F. Huang, J. Sun, S.P. Chen, M.L. Ruan, Morphology of multiple liquid phase separation in iron oxide red glaze and chemical composition of various phases, *J. Chin. Ceram. Soc.* 12 (1984) 236–242.
- [26] Britt John, Mid-range reduction glazes, *Ceram. Mon.* 11 (2009) 13–16.